Photochemical depletion of heavy CO isotopes in the Martian atmosphere

Juan Alday[1,*], Alexander Trokhimovskiy[2], Manish R. Patel[1], Anna A. Fedorova[2], Franck Lefèvre[3], Franck Montmessin[3], James A. Holmes[1], Kylash Rajendran[1], Jon P. Mason[a], Kevin S. Olsen[1,4], Denis A. Belyaev[2], Oleg Korablev[2], Lucio Baggio[3], Andrey Patrakeev[2] and Alexey Shakun[2].

[1] *School of Physical Sciences, The Open University, Milton Keynes, United Kingdom.*
[2] *Space Research Institute (IKI), Moscow, Russia.*
[3] *LATMOS/CNRS, Guyancourt, France.*
[4] *AOPP, Department of Physics, University of Oxford, Oxford, United Kingdom.*

[*] Corresponding author. E-mail address: juan.alday@open.ac.uk

Abstract

The atmosphere of Mars is enriched in heavy isotopes with respect to Earth as a result of the escape of the atmosphere to space over billions of years. Estimating this enrichment requires a rigorous understanding of all atmospheric processes that contribute to the evolution of isotopic ratios between the lower and upper atmosphere, where escape processes take place. We combine measurements of CO vertical profiles obtained by the Atmospheric Chemistry Suite onboard the ExoMars Trace Gas Orbiter with the predictions of a photochemical model and find evidence of a process of photochemistry-induced fractionation that depletes the heavy isotopes of C and O in CO ($\delta^{13}C$=-160±90‰ and $\delta^{18}O$=-20±110‰). In the upper atmosphere, accounting for this process reduces the escape fractionation factor by ~25%, suggesting that less C has escaped from the atmosphere of Mars than previously thought. In the lower atmosphere, incorporation of this ^{13}C-depleted CO fractionation into the surface could support the abiotic origin of recently found Martian organics.

1. Main text

1.1 Introduction

Numerous lines of geomorphological and mineralogical evidence suggest that liquid water was once abundant on Mars' surface[1,2], but it remains unclear what climatic conditions enabled this, or what drove the transition in the climate to the dry, low pressure atmosphere we observe today. Enrichment in the heavy isotopes of several species such as N and H suggests that atmospheric escape has been an important mechanism shaping the climate and composition of the atmosphere throughout history[3,4]. Combining measured atmospheric isotope ratios with evolution models allows the estimation of the abundance of species in the atmosphere of early Mars, which demonstrates the value of a thorough understanding of the atmospheric isotope composition[5–7].

Accurate estimations of the long-term evolution of the atmosphere from its isotope composition rely on two important quantities: measurements of the past and present isotopic ratios, and the net escape fractionation factor, which determines the efficiency of the heavy-isotope enrichment as the atmosphere escapes to space[8,9]. The most accurate measurements of the isotopic composition of C and O in the atmosphere of Mars were made by the Curiosity Rover, which showed an enrichment in the heavy isotopes in CO_2 with respect to Earth-like standards ($^{13}C/^{12}C$ = 1.046 ± 0.004 VPDB and $^{18}O/^{16}O$ = 1.048 ± 0.005

VSMOW, see Methods for definition of standards), consistent with the hypothesis of substantial atmospheric loss[10,11]. On the other hand, while the fractionation factor of several escape processes of C and O has been estimated before[5,12,13], the net escape fractionation factor, accounting for all processes from the lower atmosphere to the upper atmosphere as well, remains undetermined.

By applying this methodology to the C isotopes, the density of CO_2 in the atmosphere of early Mars has been estimated[5,14]. The escape of C at present is suggested to occur mostly in the form of hot C produced by a number of different photochemical reactions, such as the direct photodissociation of CO_2 and CO or the dissociative recombination of CO^+ [15–17]. *Hu et al.*[5] showed that the photodissociation of CO efficiently enriches the atmosphere in ^{13}C as it escapes to space, and whose contribution is an important factor for explaining the current enrichment in ^{13}C in CO_2 measured by the Curiosity Rover. However, whilst CO therefore seems to be an important species for understanding the isotopic evolution of C in the atmosphere of Mars, its present-day isotopic composition has not yet been determined.

Carbon isotopic ratios can also reveal the nature of surface-atmosphere interaction processes and mineral formation. Recently, carbon isotopic measurements by the Curiosity Rover revealed anomalously large depletions in ^{13}C ($^{13}C/^{12}C \approx 0.86$-$0.93$ VPDB) on sedimentary organics potentially associated with a possible paleosurface[18]. One of the possible explanations suggested to produce ^{13}C-depleted organic material is the photochemical reduction of CO_2 into formaldehyde (CH_2O) with CO as an intermediate. In this production, the abundance of ^{13}C in CO is suggested to be lower than that in CO_2 as a result of the differential photolysis of $^{12}CO_2$ and $^{13}CO_2$ [19], transferring its isotopic signature into formaldehyde and other organics that accumulated on the surface of Gale Crater[18]. Direct measurements of the $^{13}C/^{12}C$ in CO may therefore provide constraints on whether the photoreduction of CO_2 is the responsible mechanism for the depletion of ^{13}C on the surface organics.

The reactions that determine the abundance of CO in the atmosphere of Mars are the same as the ones controlling the long-term stability of CO_2: the photolysis of CO_2 into CO, and the posterior recombination of CO back into CO_2. The stability of CO_2 in Mars' atmosphere was at first not well understood since the photodissociation of CO_2 molecules ($CO_2 + h\nu \rightarrow CO + O$) is much faster than the recombination of the products ($CO + O + M \rightarrow CO_2 + M$). It was later realised that the stability of CO_2 is instead controlled by catalytic reactions with odd-hydrogen species ($CO + OH \rightarrow CO_2 + H$), which can convert CO into CO_2 at a much faster rate[20,21]. This reaction network not only determines the relative abundances of CO_2 and CO in the atmosphere of Mars, but also controls the relative isotopic fractionation of C and O in these species.

1.2 Results

1.2.1 Measurements of the CO isotope ratios

Here, we investigate the isotopic composition of C and O in CO using solar occultation measurements by the Atmospheric Chemistry Suite (ACS) onboard the ExoMars Trace Gas Orbiter (TGO)[22]. ACS includes three spectrometers dedicated to investigate the atmosphere using different spectral ranges: the near-infrared channel (NIR), which operates between 0.7-1.7 μm; the mid-infrared channel (MIR) operating between 2.3-4.2 μm; and the thermal infrared channel (TIRVIM), which samples the atmosphere between 0.7-17 μm. In this study, we use observations from the MIR channel, which is dedicated to solar occultation observations. For these observations, the instrument's boresight is pointed towards the Sun as it rises or sets from behind the Mars disk. By making measurements every 2.1 s, the

instrument's line-of-sight crosses the atmosphere at different tangent altitudes above the surface, allowing the reconstruction of the atmospheric vertical profiles.

ACS observations have been previously used to measure for the first time the vertical distribution of CO and its seasonal variations in the atmosphere of Mars[23,24]. Here, we use the MIR data employed by *Fedorova et al.*[23], but studying the relative abundances of $^{12}C^{16}O$, $^{13}C^{16}O$ and $^{12}C^{18}O$. In particular, we use the ACS MIR measurements obtained using the secondary grating position 6, which includes fourteen diffraction orders (236-249) encompassing a spectral range between 3950-4193 cm^{-1}. We perform the retrievals in four spectral windows in diffraction orders 239 (4012-4025 cm^{-1}), 246 (4122-4142 cm^{-1}), 248 (4158-4171 cm^{-1}) and 249 (4171-4188 cm^{-1}) (see Figure 1), to retrieve the pressure, temperature and volume mixing ratios of H_2O and the aforementioned CO isotopes (see Methods). The retrieved dataset in this study comprises all ACS MIR secondary grating position 6 observations where the four presented diffraction orders were measured, which includes 242 vertical profiles mainly measured in the second halves of Martian Year (MY) 34 (L_s = 166°-349°) and MY35 (L_s = 141°-366°). This large range of observing conditions in terms of season, local time, location and dust-activity allows a better characterisation of any potential variability in the isotopic ratios, as well as to derive more reliable estimates of the measurement uncertainties.

Figure 2 shows a summary of all $^{13}C/^{12}C$ and $^{18}O/^{16}O$ isotopic ratios in CO measured in this dataset. We observe the $^{13}C/^{12}C$ ratio to be systematically depleted in the heavy isotopes with respect to the Earth-like standard. Weighting the measurements with their corresponding uncertainties, we derive an averaged value of $^{13}C/^{12}C = 0.84 \pm 0.09$ VPDB, where the uncertainties correspond to the standard deviation of the measurements. Comparing this value to that measured in CO_2 by the Curiosity Rover, it corresponds to a depletion of $^{13}C/^{12}C$ in CO of approximately 20%. On the other hand, the $^{18}O/^{16}O$ ratio is consistent at all altitudes with the Earth-like fractionation within the measurement uncertainties. The distribution of measured values in this case yields a weighted average isotopic ratio of $^{18}O/^{16}O = 0.98 \pm 0.11$ VSMOW, which compared to the isotopic ratio measured in CO_2 by the Curiosity Rover corresponds to a depletion of the O isotopic ratio in CO of 6%, although this depletion lies within the reported uncertainties from the ACS measurements.

1.2.2 Modelling the CO photochemical fractionation

In order to understand the physical and chemical processes that give rise to the depletion of the C and O isotopic ratios measured in CO, we constructed a one-dimensional photochemical model to simulate the isotopic fractionation between CO and CO_2. In particular, we include isotope-specific rates for the two most important reactions relating these two species: the photolysis of CO_2 into CO + O, and the recombination of CO + OH back into CO_2. The photolysis cross-sections for $^{12}C^{16}O_2$, $^{13}C^{16}O_2$ and $^{18}O^{12}C^{16}O$ are taken from *Schmidt et al.*[19] (see Extended Data Figures 1 and 2), while the fractionation during the recombination of CO into CO_2 is modelled using data from laboratory measurements[25] (see Extended Data Figure 3). This photochemical model extends from the surface up to an altitude of 200 km and is set to represent Martian mean dayside conditions (i.e., solar zenith angle equal to 60° and Sun-Mars distance of 1.52 AU[26]). The isotopic ratios in the model are initialised following the measurements from the Curiosity Rover, and the model is then run for approximately 20 years, the time by which the isotopic ratios in CO and CO_2 have converged to a steady-state solution (see Extended Data Figure 4).

Figure 3 shows the derived C isotopic abundances from the photochemical model, together with the measured values from the ACS observations. The C isotopic ratios in both CO and CO_2 show a similar altitudinal trend above approximately 100 km, where they continuously

decrease with increasing altitude due to diffusive separation: above the homopause, where molecular diffusion dominates, species are mixed according to their own mass-dependent scale height. As a result of this, the isotopic ratios steadily decrease with altitude, with the decrease in $^{13}C/^{12}C$ being approximately half of $^{18}O/^{16}O$ [27] (see Extended Data Figure 4). While the isotopic ratios in CO_2 below the homopause altitude are approximately constant, those in CO are depleted in the heavy isotopes due to photochemistry-induced fractionation, mainly due to the preferential photolysis of $^{12}C^{16}O_2$ over $^{13}C^{16}O_2$ and $^{18}O^{12}C^{16}O$ (see Extended Data Figures 1 and 2). In particular, the photochemical model suggests that below 30 km the C isotopic ratio in CO is approximately 24% lower than in CO_2, increasing to about 9% at 100 km. The effect of the photochemistry has a smaller impact in the O isotope ratios, with the depletion of the heavy isotopes near the surface being approximately 9%. Although the ACS measurement uncertainties in the $^{18}O/^{16}O$ isotopic ratio are large compared with the magnitude of the photochemistry-induced fractionation, the lower value of the $^{13}C/^{12}C$ ratio in CO than that in $^{18}O/^{16}O$ predicted by the photochemical model is consistent with the ACS measurements presented in this study.

1.3 Discussion

Both the ACS measurements and the predictions from the model suggest that the photochemistry of the atmosphere of Mars produces a depletion of the heavy C and O isotopes in CO. Isotopic fractionation also occurs during the photolysis of other species such as H_2O, whose effect in the Martian atmosphere has been extensively studied[28,29]. The photolysis-induced fractionation in H_2O is responsible for fractionating the D/H ratio in water, molecular hydrogen, and finally the escaping products, giving rise to an efficient enrichment in D/H as the atmosphere escapes to space[29–31].

Since CO contributes a substantial fraction of the C escape from Mars, this source of fractionation has to be accounted for when estimating the net escape fractionation factor. The escape of C from the atmosphere of Mars due to CO photodissociation and photoionisation is most efficient at altitudes above 150 km[15,17]. At these altitudes, the isotopic composition of CO is affected by both the chemistry and diffusive separation. Our model suggests that at 200 km, the $^{13}C/^{12}C$ isotopic ratio in CO is ~0.75 times that of the bulk atmosphere, which combined with the fractionation factor due to escape by CO photodissociation ($\alpha \approx 0.6$ [5]) yields a net escape fractionation factor of ~0.45 for this reaction. This lower fractionation factor indicates that the C escape through CO photodissociation enriches the atmosphere in ^{13}C more efficiently than previously thought, requiring less C escape to explain the present-day enrichment of ^{13}C in CO_2 in the atmosphere of Mars.

Based on a primordial isotopic ratio of $^{13}C/^{12}C = 0.975$ VPDB [32] and the current isotopic enrichment in CO_2 from the Curiosity Rover, *Hu et al.*[5] estimated that an equivalent pressure of 240 mbar of C was lost to space throughout history, with photochemical escape being the dominant escape mechanism in the last 1.5 billion years (~8 mbar), and sputtering of CO_2 being dominant earlier in history (~232 mbar). While the photochemistry-induced fractionation impacts only the photochemical escape fractionation factor, it can have implications to the overall estimated escape rates depending on the relative contributions from both mechanisms. On one hand, the lower escape fractionation factor derived in this study might indicate that photochemical escape has contributed less than previously thought to the overall escape rates (i.e., <8 mbar). On the other hand, it might indicate that the contribution from sputtering may have been overestimated (i.e., <232 mbar) by a larger fraction than in the previous case, given the low efficiency of the sputtering process in enriching the atmosphere in ^{13}C[33].

The photochemistry in Mars' atmosphere therefore favours a preferential transfer of $^{13}C/^{12}C$ from CO to CO_2, decreasing the total amount of $^{13}C/^{12}C$ in CO and transferring it to CO_2, subsequently increasing the $^{13}C/^{12}C$ isotopic ratio of this species. However, given the orders-of-magnitude difference between the abundances of CO and CO_2 in the atmosphere of Mars, while the transfer of $^{13}C/^{12}C$ from CO to CO_2 produces a substantial effect on the overall isotopic ratio of CO, the effect on that of CO_2 is minimal. In particular, we find the near-surface isotopic ratio in CO_2 to be 0.004% higher than that in the initial atmosphere, which corresponds to an enrichment of $\delta^{13}C \approx 0.04$ ‰. This value is much smaller than the enrichment in the heavy isotopes observed by the Curiosity Rover ($\delta^{13}C = 46 \pm 4$ ‰ [10]), which suggests that atmospheric escape remains as the preferred process contributing to the enrichment of ^{13}C in the atmosphere of Mars.

The depletion of ^{13}C in CO observed with the ACS measurements and predicted by the photochemical model is in line with the measurements of the $^{13}C/^{12}C$ ratio in Martian organics made by the Curiosity Rover[18]. While other suggested formation mechanisms such as the photolysis of CH_4 released from the subsurface or the deposition of cosmic dust cannot be ruled out as responsible for the production of ^{13}C-depleted organics on Mars, our results confirm that the photolysis of CO_2 can produce strong depletions of the $^{13}C/^{12}C$ ratio in CO, an isotopic signature that can be transferred to formaldehyde or other organics that might accumulate on the surface of Mars.

The photochemical model also predicts a relative depletion of the $^{18}O/^{16}O$ isotopic ratio in CO with respect to CO_2, although to a lesser extent than for the C isotopes. The implications of this source of fractionation to the long-term evolution of the O isotopes are nevertheless more complicated due to the much more complex O chemistry in the atmosphere of Mars. The dissociative recombination of O_2^+, responsible for most of the O escape from Mars[34], also efficiently enriches the atmosphere in ^{18}O as escape occurs[13]. However, the overall escape fractionation factor will be subject to the $^{18}O/^{16}O$ ratio in O_2^+ and the source species of these ions (i.e., O, O^+, CO_2, CO_2^+ [35]), which will likely be affected by the isotope photochemistry. Based on the isotope-specific photolysis cross-sections included in this study, while the O isotopic ratios of CO_2 in the ionosphere will mostly be affected by the diffusive separation above the homopause, the isotopic composition of atomic O will be affected by the preferential photolysis of $^{12}C^{16}O_2$ over $^{18}O^{12}C^{16}O$, similar to the observed depletion of $^{18}O/^{16}O$ in CO. However, since atomic O is produced and lost in several other chemical reactions, a comprehensive analysis of the O isotopic composition in the upper atmosphere requires a model accounting for ^{18}O in other species, which is planned but beyond the scope of the work presented here.

The results from this study highlight the important role of photochemistry in fractionating the C and O isotopic composition of the atmosphere of Mars. Future measurements of the isotopic ratios in different species may not only provide key information about the photochemical cycles in the atmosphere of Mars, but also provide accurate estimations of the fractionation between the lower and upper atmospheres, which has important implications to our understanding of the long-term evolution of Mars' climate.

2. Methods

2.1 Retrieval scheme

The inversion of the spectra is performed using the NEMESIS algorithm[36], applying the same two-step methodology as in *Alday et al.*[37]. First, the pressure and temperature profiles are determined using the CO_2 absorption features in diffraction order 239 (see Figure 1). Secondly, the pressure and temperature are fixed, and the abundances of the trace gases

(i.e., H_2O, $^{12}C^{16}O$, $^{13}C^{16}O$ and $^{12}C^{18}O$) are retrieved using all diffraction orders. All gaseous absorption in this study is modelled using pre-computed line-by-line look-up tables generated using the spectroscopic parameters from the 2020 edition of the HITRAN database[38]. Apart from the retrieval of the atmospheric parameters, the instrument line shape (ILS) is also fitted in each occultation using a double Gaussian parameterisation [39].

The pressure and temperature profiles are retrieved under the assumption of an atmosphere in hydrostatic equilibrium and a known CO_2 volume mixing ratio. This approach has been widely used in the past to determine the thermal structure of the atmosphere of Mars from solar occultation observations [40]. The retrieval scheme from the NEMESIS algorithm works using the optimal estimation framework, which aims to find an optimal solution that is consistent with the observed spectra subject to a minimal departure from the *a priori*. Given that the absorption features of CO_2 measured in ACS MIR secondary grating position 6 typically disappear at lower tangent altitudes than the CO ones, we use temperature profiles from simultaneous observations by ACS NIR [23] as the *a priori* in our retrievals, which ensures an accurate description of the temperature field at all altitudes. The use of accurate measurements of temperature is crucial to derive precise measurements of the CO isotopic ratios, which are highly sensitive to this parameter (see Supplementary Figure 1).

Once the pressure and temperature profiles are determined, these are fixed, and the gaseous abundances of the CO isotopes and H_2O are retrieved. In this case, the *a priori* information is taken from the OpenMARS reanalysis dataset[41], which assimilates the temperature profiles and dust opacities measured by the Mars Climate Sounder onboard the Mars Reconnaissance Orbiter into the General Circulation Model. The *a priori* isotopic composition is assumed to follow that of Earth-like conditions given by the Vienna Pee Dee Belemnite ($^{13}C/^{12}C$ = 1 VPDB = 0.0112372) and the Vienna Standard Mean Ocean Water ($^{18}O/^{16}O$ = 1 VSMOW = 0.0020052). Given that the sensitivity of the retrieval to the CO isotopes can be different at different altitudes (i.e., the $^{12}C^{18}O$ absorption lines typically disappear at lower tangent heights than the $^{12}C^{16}O$), the influence of the *a priori* guess in the retrieval of the isotopologues might also be different. Therefore, in order to ensure no biases from the *a priori* are introduced into the derivations of the isotopic ratios, the retrievals are run twice, the second time using the retrieved $^{12}C^{16}O$ abundances from the previous iteration as the *a priori* and scaling the abundances of the minor isotopes with the same Earth-like isotopic ratios.

In each acquisition made by ACS MIR, the observed diffraction orders encompass about 20 detector rows, which correspond to the instantaneous field-of-view of the instrument, with each row sampling slightly different tangent heights ($\Delta z \approx 150$ m per row). In addition, the ILS varies from row to row, which can introduce systematic uncertainties in the retrievals. In order to increase the confidence of the retrievals and better understand the uncertainties arising from the ILS fitting, we apply the retrieval scheme to seven detector rows. The retrieved profiles from each row are then combined using a weighted average based on the retrieved uncertainties. The uncertainties are calculated considering both the error of the mean, and the standard deviation of the profiles[27]. We consider this method for calculating the uncertainties to provide a more accurate representation of the true uncertainty of the retrieval in which not only the random uncertainties, but also the systematic ones are captured.

2.2 Sensitivity of the measured isotopic ratios to the temperature field

The spectroscopic parameters tabulated in line databases such as HITRAN[38] depend on the atmospheric temperature. The dependence of these spectroscopic parameters to the temperature are different for each absorption line and gas, which might create systematic biases in the retrieval of the gaseous abundances and isotopic ratios if the temperature is

not known. In order to determine the sensitivity of our retrievals to the temperature distribution, we perform a series of retrievals of the isotopic ratios in CO using different temperature profiles. In particular, we retrieve the abundances of $^{12}C^{16}O$, $^{13}C^{16}O$ and $^{12}C^{18}O$ from the spectral windows in diffraction orders 246, 248 and 249 (see Figure 1) under three assumptions: the temperature profiles are given by those derived from simultaneous measurements by ACS NIR[23], and adding a constant offset of ±5 K. These retrievals are performed for the first 20 orbits of ACS MIR measurements with secondary grating position 6 (orbits 1853-2530).

Supplementary Figure 1 summarises the results from this experiment, showing the weighted averaged profiles of the isotopic ratios from these retrievals. These results indicate that the $^{13}C/^{12}C$ and $^{18}O/^{16}O$ ratios are highly sensitive to the temperature field: an offset of 5 K in the temperature field introduces a bias of 15-20% in the retrieved isotopic ratios. It must be noted that this kind of bias is not random but systematic, meaning that a constant offset in the assumed temperature field always leads to a bias in the isotopic ratios in the same direction. On the contrary, Supplementary Figure 1 shows that a temperature offset of 5 K only produces deviations of 1-2% in the ratio between the abundances of $^{13}C^{16}O$ and $^{12}C^{18}O$. This indicates that it is indeed the retrieval of $^{12}C^{16}O$ that is most affected by inaccuracies in the temperature, and the ratio between the abundances of the minor isotopes is a useful magnitude to better interpret the analysis of the isotopic ratios in this study.

2.3 Validation of the retrieved vertical profiles

Simultaneous measurements made by the NIR and MIR channels on ACS provide a unique opportunity to validate the measurements from both channels. Numerous validation exercises have been performed in previous studies, focusing on the retrievals from different spectral ranges or ACS MIR secondary grating positions[23,37,42]. In particular, *Fedorova et al.*[23] used all three ACS channels to validate the retrievals of the CO abundances from secondary grating position 6, data which is used in the present study. Here, we perform a similar exercise, but including comparisons of simultaneous measurements of temperature too.

The temperature retrieval is the first step of the retrieval scheme presented in this study. We use the temperature profiles from the simultaneous ACS NIR channel measurements as the *a priori* in our retrievals, given that the temperature retrievals from that channel can extend to higher altitudes than the ones derived from secondary grating position 6. In order to validate the retrievals of the temperature from both channels and ensure that the temperatures derived in this study are driven by the data and not the prior information, we perform a series of tests using the measurements made during the first 20 orbits. In these test retrievals, we select a prior profile given by the ACS NIR temperature profile with an offset of ±10 K.

Supplementary Figure 2 shows an example of the results for the first three measurements. These figures highlight that the retrieved temperature profiles below ≈55 km from ACS MIR are driven by the measured data and are not sensitive to the assumed *a priori* profiles. Above this altitude, where there is no information in the spectra, the retrieved profiles tend to their respective *a priori*. Using the ACS NIR profiles as the *a priori* guess in our retrieval scheme ensures that the retrieved profiles from ACS MIR will also be accurate above this altitude, where we can still measure the abundances of the CO isotopes.
Once the temperature profiles are retrieved, these are fixed, and the gaseous abundances of the CO isotopologues are retrieved using order 246, 248 and 249. Supplementary Figure 3 provides a general overview of the comparison between the ACS NIR and MIR datasets, showing the differences in retrieved abundances and temperatures. The differences between both channels are on average centred on zero, considering that different absorption

bands are used and the uncertainties of the retrievals, which indicates that there are no strong systematic differences between both datasets.

Finally, once the retrieved abundance of the CO isotopes is determined, the isotopic ratios are derived. In order to ensure that our measurements and conclusions about the isotopic ratios are robust, we compare the retrieved isotopic ratios when using the temperature profiles from the NIR and MIR channels during the first 20 orbits (see Supplementary Figure 4). We find that when using either dataset, we would draw similar conclusions: the $^{13}C/^{12}C$ ratio is depleted with respect to the standard, while the $^{18}O/^{16}O$ ratio is consistent with a value of 1 VSMOW within the retrieved uncertainties. The ratio between the two (i.e., $^{13}C^{16}O/^{12}C^{18}O$), not dependent on the temperature field, provides a robust confirmation that the depletion of ^{13}C in CO is real.

It can be observed in Supplementary Figure 4 that the vertical profiles of the $^{13}C/^{12}C$ and $^{18}O/^{16}O$ isotopic ratios show a sudden increase below 20 km when fixing the temperature profiles from the ACS NIR channel. The magnitude of the increase is equal for both isotopic ratios, which is evidenced by the lack of such an increase in the ratio between $^{13}C^{16}O/^{12}C^{18}O$. This sudden increase of the isotopic ratios towards the surface could be caused by an unknown process that fractionates both isotopologues equally (i.e., $\delta^{13}C = \delta^{18}O$). However, a more plausible explanation is that they are the result of a bias in the retrievals at these lowest altitudes in their common factor, the abundance of $^{12}C^{16}O$. In particular, the increasingly abundance of dust towards the surface negatively impacts the sensitivity of the measurements to the gaseous abundances and the temperature field. As it is shown in Supplementary Figure 1, a bias of temperature field of just a few Kelvins can lead to substantial differences in the retrieved abundance of $^{12}C^{16}O$, while the retrieval of the minor isotopes is more insensitive to such deviations. Such a bias in the abundance of $^{12}C^{16}O$ at the lowest altitudes can lead to equal deviations in the calculation of the $^{13}C/^{12}C$ and $^{18}O/^{16}O$ isotopic ratios, following $\delta^{13}C = \delta^{18}O$.

The simultaneous retrieval of the temperature field and the abundances of the CO isotopes with the ACS MIR channel mostly mitigates the bias found in the lowest altitudes (see Supplementary Figure 4). However, the reduced sensitivity of the measurements at these altitudes due to the presence of dust can lead to a similar but smaller systematic behaviour in our retrieval scheme. Supplementary Figure 5 shows the averaged profiles of $^{13}C/^{12}C$ and $^{18}O/^{16}O$ in CO derived from the whole ACS MIR dataset used in this study. Although substantially lower than the reported uncertainties, both the C and O isotopic ratios appear to increase below 15 km towards the surface. The relationship between both isotopic ratios at these altitudes follows $\delta^{13}C = \delta^{18}O$, which suggests that this feature is not real, but caused by a systematic bias in the retrievals. Since the reality of such feature is questionable based on the discussion above, we currently refrain from including the measurements at these altitudes and its potential science implications until we investigate this further with other ACS MIR measurements in other spectral ranges.

2.4 Photochemical model

The 1D photochemical model aims to solve the continuity equation given by

$$\frac{\partial n_i}{\partial t} = P_i - L_i - \frac{\partial \phi_i}{\partial z},$$

where n_i is the number density of a given species, P_i and L_i represent the production and loss of density due to the photochemical reactions, and the last term represents the diffusion

between layers, where ϕ is the flux. The flux is calculated considering both Eddy and molecular diffusion and is given by

$$\phi_i = -(K + D_i)\frac{\partial n_i}{\partial z} - n_i\left[K\left(\frac{1}{H_0} + \frac{1}{T}\frac{\partial T}{\partial z}\right) + D_i\left(\frac{1}{H_i} + \frac{(1+\alpha)}{T}\frac{\partial T}{\partial z}\right)\right],$$

where K and D_i are the Eddy and molecular diffusion coefficients, H_0 is the mean scale height, H_i is the gas-dependent scale height, α is the thermal diffusion coefficient, and T is the temperature.

The diffusion term is calculated by finite differences[43], which yields

$$\frac{\partial \phi_{i,j}}{\partial z} \sim -\left(k_j + d_{i,j}\right)\cdot n_{i,j+1} + \left(kl_j + dl_{i,j} + k_{j-1} + d_{i,j-1}\right)\cdot n_{i,j} - \left(kl_{j-1} + dl_{i,j-1}\right)\cdot n_{i,j-1}$$

where the subscripts i and j represent the gas and layer, respectively. The coefficients in the finite differences approximation are given by

$$k_j = \frac{K_{j+1/2}}{\Delta z^2},$$

$$d_{i,j} = \frac{D_{i,j+1/2}}{\Delta z^2},$$

$$kl_j = k_j \cdot \left(1 - \frac{\Delta z}{H_{0_{j+\frac{1}{2}}}} - \frac{T_{j+1} - T_j}{T_{j+\frac{1}{2}}}\right),$$

$$dl_{i,j} = d_{i,j} \cdot \left(1 - \frac{\Delta z}{H_{i,j+\frac{1}{2}}} - (1+\alpha)\cdot\frac{T_{j+1} - T_j}{T_{j+\frac{1}{2}}}\right),$$

where Δz is the altitude of each layer.

The production and loss terms are calculated using the latest version of the photochemical scheme from the Mars Planetary Climate Model (PCM) , which has been extensively used to model the photochemical cycles in the atmosphere of Mars[44–46]. This scheme includes 14 chemical species and 39 chemical reactions to model the photochemistry of H, C and O in the atmosphere of Mars. Here, we introduce four new species ($^{13}C^{16}O_2$, $^{13}C^{16}O$, $^{18}O^{12}C^{16}O$ and $^{12}C^{18}O$) and eleven chemical reactions to model the isotopic fractionation between CO_2 and CO. The reaction rates are calculated assuming mean dayside conditions with a constant solar zenith angle of 60° and a constant Sun-Mars distance of 1.52 AU.

The reactions included to model the ^{13}C chemistry are:

$^{13}CO_2 + hv \rightarrow {}^{13}CO + O$ (λ > 167 nm)
$^{13}CO_2 + hv \rightarrow {}^{13}CO + O(^1D)$ (λ < 167 nm)

$^{13}CO + O + M \rightarrow {}^{13}CO_2 + M$

$^{13}CO + OH \rightarrow {}^{13}CO_2 + H$

The reactions included to model the O fractionation between CO_2 and CO are:

$^{18}OC^{16}O + hv \rightarrow C^{18}O + {}^{16}O$ ($\lambda > 167$ nm)
$^{18}OC^{16}O + hv \rightarrow C^{16}O + {}^{16}O$ ($\lambda > 167$ nm)

$^{18}OC^{16}O + hv \rightarrow C^{18}O + {}^{16}O(^1D)$ ($\lambda < 167$ nm)
$^{18}OC^{16}O + hv \rightarrow C^{16}O + {}^{16}O(^1D)$ ($\lambda < 167$ nm)

$C^{18}O + {}^{16}O + M \rightarrow {}^{18}OC^{16}O + M$

$C^{18}O + {}^{16}OH \rightarrow {}^{18}OC^{16}O + H$
$C^{16}O + {}^{18}OH \rightarrow {}^{18}OC^{16}O + H$

It must be noted that in the version for the ^{18}O chemistry the total mass is not conserved, as we do not include ^{18}O or $^{18}O(^1D)$ in the chemistry scheme. The only ^{18}O-bearing species included in the model apart from CO and CO_2 is ^{18}OH, whose isotopic ratio is fixed throughout the simulation to follow that measured by the Curiosity Rover in CO_2, and whose recombination with $C^{16}O$ is assumed to produce no isotopic fractionation. Inclusion of all ^{18}O-bearing species would be required to model the complete chemistry of ^{18}O in the atmosphere of Mars. However, here we restrict our analysis to model the relative fractionation of the $^{18}O/^{16}O$ isotopic ratio between CO_2 and CO, which is not expected to be affected by this simplification, since CO molecules are solely produced by the photolysis of CO_2, which is included in the scheme.

The continuity equation is solved using a second-order Rosenbrock algorithm[47,48]. The density at the next time step is calculated following

$$n^{t+1} = n^t + 1.5\Delta t \cdot g_1 + 0.5\Delta t \cdot g_2,$$
$$(I - \gamma \Delta t J) g_1 = f(n^t),$$
$$(I - \gamma \Delta t J) g_2 = f(n^t - \Delta t g_1) - 2g_1,$$

Where $\gamma = 1 + 1/\sqrt{2}$, Δt is the time step, $f(n)$ is the right-hand side of the differential equation (i.e., the chemistry and transport terms evaluated at the density n) and J is the Jacobian matrix of the combined chemistry-transport system. Since the densities of a given species at a given layer are only influenced by the densities of the other gases in the same layer (i.e., chemistry) and the densities of the same gas in the adjacent layers (i.e., diffusion), the Jacobian matrix takes the form of a block tridiagonal matrix, which is efficiently inverted using the Thomas algorithm.

The choice of the time step is made based on the maximum local error, which is estimated by the difference between the first-order and second-order solutions, following

$$\varepsilon = n^{t+1} - n_1^{t+1} = (n^t + 1.5\Delta t \cdot g_1 + 0.5\Delta t \cdot g_2) - (n^t + \Delta t \cdot g_1).$$

The timestep is self-adjusted by $\Delta t^{t+1} \sim \Delta t^t / \sqrt{\varepsilon_{max}}$, which ensures that the convergence of the system to a steady-state solution will capture the orders-of-magnitude difference in the chemical and diffusion timescales while optimising the computational time.

The 1D photochemical model requires several inputs to represent the composition and mixing of the atmosphere of Mars. The initial temperature and density profiles are derived using an average of vertical profiles generated from the 'standard climatololgy' scenario of the Mars Climate Database v6.1[49] at different times and locations. In particular, we generate vertical profiles of temperature and gas number densities from 0 to 200 km in a grid of latitudes, local times and solar longitude L_S. The latitudes expand from -80° to 80° with a

step of 20°. The local time expands from 0 to 24 hours with a two-hour step. The L_S expands the whole year, with a step of 10°. The calculated profiles are then averaged to initialise the vertical profiles in the one-dimensional model (see Supplementary Figure 6). The abundances of CO_2 and CO from the Mars Climate Database are then divided into the different isotopologues by assuming a given isotopic ratio, and using

$$[^{12}C^{16}O_2] = [CO_2] / (1 + R)$$
$$[^{13}C^{16}O_2] = [^{12}C^{16}O_2] \times R$$

where the bracketed quantities represent the abundances of the different species, and *R* is the isotopic ratio measured in CO_2 with the Curiosity Rover (i.e., $^{13}C/^{12}C$ = 1.046 VPDB and $^{18}O/^{16}O$ = 1.048 VSMOW[10]).

The diffusion coefficients assumed in our Mars 1D photochemical model are the same as those used by *Cangi et al.*[30], which were taken from other previous studies[43,50]. In particular, the Eddy diffusion coefficient is given by

$K(z \leq 60\ km) = 10^6$ cm^2 s^{-1},
$K(z > 60\ km) = 2 \cdot 10^{13} \cdot n(z)^{-1/2}$ cm^2 s^{-1},

as shown in Supplementary Figure 6. The molecular diffusion coefficient is given by

$$D(z) = \frac{AT(z)^s}{n(z)}.$$

The coefficients *A* and *s* for H_2 and H are equal to $A_H = 8.4 \times 10^{17}$, $s_H = 0.597$, $A_{H2} = 2.23 \times 10^{17}$, $s_{H2} = 0.75$ [50]. For the rest of the species, we adopt $A = 10^{17}$ and $s = 0.75$ (see Supplementary Figure 6).

The boundary conditions are similar to those used in previous studies[51]. We consider the top boundary conditions to be a zero flux for all species but for H_2, H and O. For H_2 and H, we fix their escaping velocities to be $v_{H2} = 3.4 \times 10^1$ cm s^{-1} and $v_H = 3.1 \times 10^3$ cm s^{-1}, while for O we fix the escaping flux to be $\phi_O = 1.2 \times 10^8$ cm^{-2} s^{-1}. For the lower boundary conditions, we set a zero flux for all species, but for H_2O, whose density is assumed to be fixed below 50 km.

Using these inputs and the presented model setup, we run a simulation for 20 years, the time by which the O and C isotopic ratios in both CO and CO_2 have converged to a steady-state solution, as it is shown in Extended Data Figure 4.

2.5 Fractionation during the photolysis of CO_2

The photolysis cross sections of CO_2 used in the chemistry scheme of the LMD Mars PCM are a composite of different laboratory measurements in different spectral ranges[52–56] and tabulated at temperatures of 195, 295 and 370 K [44]. In order to model the fractionation factor of this reaction, we use the photolysis cross sections calculated by *Schmidt et al.*[19] for $^{12}C^{16}O_2$, $^{13}C^{16}O_2$ and $^{18}O^{12}C^{16}O$ between 150-210 nm, which are combined with the Mars PCM reference for <150nm at 195, 295 and 370 K. Extended Data Figure 1 shows how the calculated cross sections for $^{12}C^{16}O_2$ compare with those tabulated in the chemistry scheme, together with a comparison between the cross sections calculated for the different isotopologues. These results suggest that the photolysis cross sections of $^{12}C^{16}O_2$ are larger than those of the minor isotopes (i.e., $^{13}C^{16}O_2$ and $^{18}O^{12}C^{16}O$) by a factor of 1.0-1.5 and 1.0-1.3, respectively. The ratio between the cross sections of $^{12}C^{16}O_2$ and those of the minor

isotopes also depends on the temperature, with that at 195 K being on average 5% larger than that at 295 K.

It is important to note that the cross sections for the minor isotopes are only available for a limited spectral range (>150 nm), and these are lower than the cross sections elsewhere (<150 nm), where we assume that they are equal for all isotopes. In order to evaluate where the cross sections >150 nm are most effective in the photolysis of CO_2 molecules in the atmosphere of Mars, we calculate the photolysis *J*-values as a function of altitude (see Extended Data Figure 2). These results show that the *J*-values are approximately constant above ≈100 km, where the atmosphere is optically thin. Below this altitude, the atmosphere becomes optically thick for wavelengths lower than 150 nm, and the *J*-values decrease with decreasing altitude as the atmosphere also becomes optically thick for wavelengths >150 nm. Therefore, while the cross sections <150 nm are important above 100 km, their effect becomes negligible below 100 km, the region where the ACS observations can measure the isotopic fractionation between CO_2 and CO.

Panel b on Extended Data Figure 2 shows the ratio between the photolysis rates of $^{12}C^{16}O_2$ over those of $^{13}C^{16}O_2$ and $^{18}O^{12}C^{16}O$, which is higher than one at all altitudes. These results suggest that the photolysis of $^{12}C^{16}O_2$ is faster than that of the minor isotopes, meaning that $^{12}C^{16}O$ will be more efficiently produced than $^{13}C^{16}O$ and $^{12}C^{18}O$. The net effect of this process is to produce a depletion of the $^{13}C/^{12}C$ and $^{18}O/^{16}O$ ratios in CO with respect to those in CO_2, and the magnitude of this effect is larger for the C isotopes than the O ones.

2.6 Fractionation during the recombination of CO + OH

The recombination of CO with the hydroxyl radical OH is an important reaction in the chemistry of the atmosphere of Mars, which is responsible for the stability of CO_2 [20,21]. In order to model the isotopic fractionation of the C and O isotopes in this reaction, we use the data derived from laboratory measurements[25]. These measurements determined the kinetic isotope effect at a range of pressures from 0.2 to 1.35 atm (see Extended Data Figure 3). In order to extrapolate the measurements to the low pressure of the Martian atmosphere, we fit this dependence using a second-order polynomial function. The fitted polynomial functions for the C and O isotopes are respectively

$$k^{13}/_{k^{12}} = 1.00638 - 1.69300 \times 10^{-7} \cdot p + 4.69677 \times 10^{-13} \cdot p^2,$$
$$k^{18}/_{k^{12}} = 1.01195 - 4.44340 \times 10^{-7} \cdot p + 1.93835 \times 10^{-13} \cdot p^2,$$

where the ratios $^{13}k/^{12}k$ and $^{18}k/^{16}k$ represent the ratio between the reaction rates of the minor isotopes (i.e., ^{13}CO and $C^{18}O$) with respect to that of the major one (i.e., $^{12}C^{16}O$) and *p* is the pressure in Pascals.

At the low pressures of the Martian atmosphere, this reaction is faster for the minor isotopes, which yields a preferential transfer of ^{13}C and ^{18}O over ^{12}C and ^{16}O from CO to CO_2. Therefore, the net effect of this reaction is to produce a depletion of the $^{13}C/^{12}C$ and $^{18}O/^{16}O$ isotopic ratios in CO with respect to CO_2. However, given the small magnitude of this fractionation factor with respect to that produced by the photolysis of CO_2, this process is expected to have a much minor effect in the overall fractionation between CO_2 and CO.

3. Data availability

The datasets generated by the ExoMars Trace Gas Orbiter instruments analysed in this study are available in the ESA Planetary Science Archive (PSA) repository, https://archives.esac.esa.int/psa, following a six months prior access period,

following the ESA Rules on Information, Data and Intellectual Property. The data products generated in this study (retrieved atmospheric parameters) can be downloaded from a Zenodo repository[57].

4. Code availability

The spectral fitting and retrievals were performed using the NEMESIS radiative transfer and retrieval algorithm, which can be downloaded from a Zenodo repository[58]. The photochemical code used to model the isotopic fractionation in the atmosphere of Mars can be downloaded from a Zenodo repository[59]. Interested users are encouraged to contact the corresponding author for the usage of these tools.

5. Acknowledgments

The authors thank the reviewers, Vladimir A. Krasnopolsky and Daniel Y. Lo, for their useful criticism and suggestions for improvement. The authors thank Nick Thomas, Matthew Read (University of Bern), Charlotte Marriner (The Open University) and the TGO/CaSSIS team for providing supporting images. The authors thank Begoña Alday for providing a supporting animation for outreach purposes. The ExoMars mission is a joint mission of the European Space Agency (ESA) and Roscosmos. The ACS experiment is led by the Space Research Institute (IKI) in Moscow, assisted by LATMOS in France. This work was funded by the UK Space Agency and Science and Technology Facilities Council (ST/Y000234/1, ST/V002295/1, ST/V005332/1 and ST/X006549/1), Roscosmos, the National Centre for Space Studies of France (CNES) and the Ministry of Science and Education of Russia. Science operations are funded by Roscosmos and ESA.

6. Competing interests

The authors declare no competing interests.

7. Author contributions

Atmospheric retrievals from the ACS MIR spectra and interpretation of the retrieved parameters were performed by J.A. A.T., M.R.P, A.A.F., F.M., J.P.M., K.S.O, D.A.B. and O.K. provided input and help with spectral fitting and retrievals. Processing of the spectra was done by L.B. at LATMOS and by A.T. at IKI. F.L., M.R.P., J.A.H and K.R. provided input into the development of the photochemical model. The ACS instrument was operated by A.T., A.P. and A.S. All co-authors contributed to the preparation of the manuscript.

8. Figures

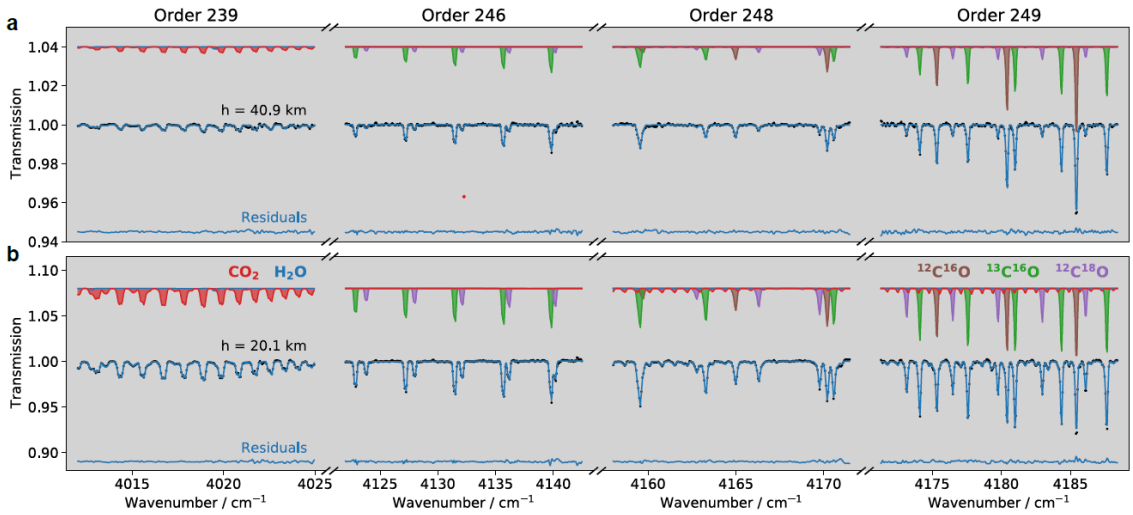

Figure 1: Example of ACS MIR spectra from secondary grating position 6*. The panels show the measured transmission spectra in four diffraction orders (black dots) made during orbit 1896 (Latitude = 83.8°; Longitude = 170.5°; L_s = 166°; Local time = 22.5 h) and best fit (blue lines) at 20 (b) and 40 km (a). The residuals between the measurement and best fit in each diffraction order are shown in each panel, together with the contribution from each gas to each spectrum, adding a constant offset in both to improve the visibility of the figure.*

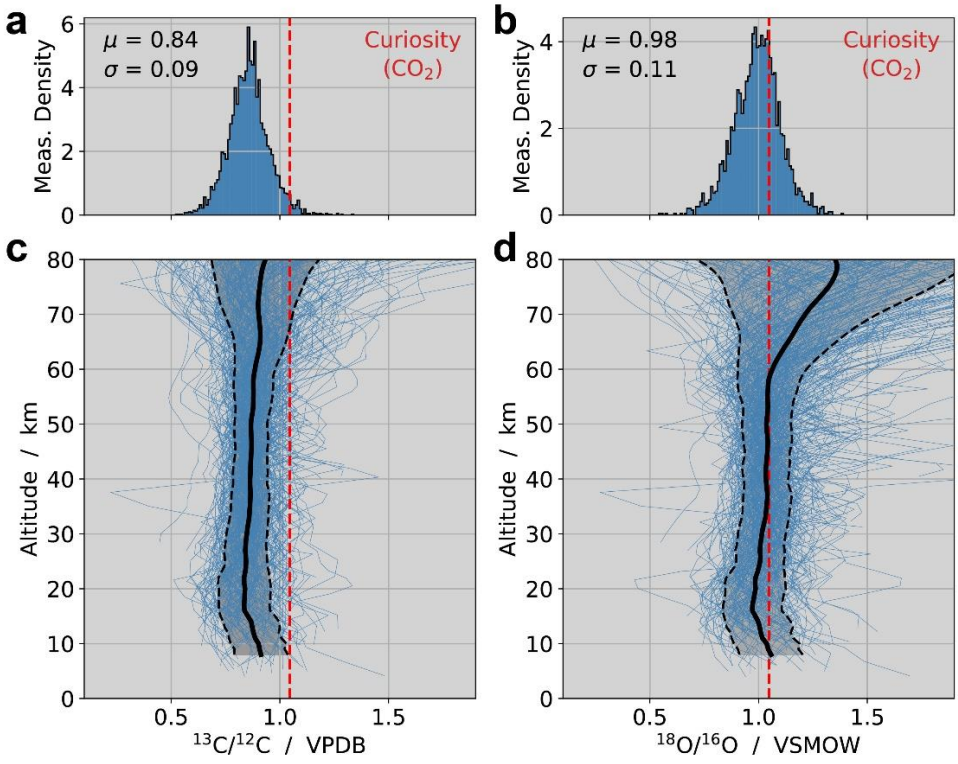

Figure 2: Vertical profiles of the C and O isotopic ratios in CO in the atmosphere of Mars. *Panels a and b show the histogram of all measured $^{13}C/^{12}C$ and $^{18}O/^{16}O$ ratios in standard units with uncertainties lower than 0.4. Panels c and d show the 242 measured vertical profiles of the isotopic ratios in this dataset (blue thin lines), as well as the weighted average (black line) and the standard deviation of the profiles (shaded areas). The red lines indicate the isotopic ratios in CO_2 measured by the Curiosity Rover in standard units given by Vienna Pee Dee Belemnite (VPDB) and Vienna Standard Mean Ocean Water (VSMOW).*

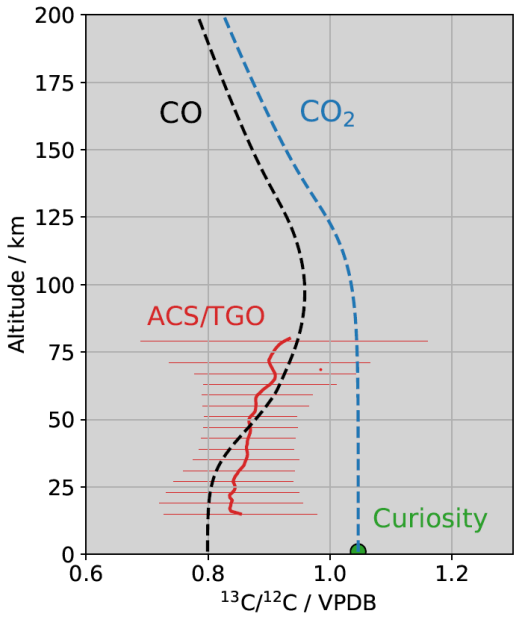

Figure 3: Photochemistry-induced fractionation of the C isotopes in the atmosphere of Mars. *The ACS measurements (red) reveal a decrease of the $^{13}C/^{12}C$ isotope ratio in CO larger than the measured uncertainties (horizontal red lines) with respect to that in CO_2 measured by the Curiosity Rover at the surface (green). The predictions from the 1D photochemical model (dashed lines) suggest that this decrease is produced by the chemistry of the Martian atmosphere, which preferentially favours the transfer of ^{13}C from CO (black) to CO_2 (blue). The isotope ratio in CO in the upper atmosphere, responsible for a substantial fraction of the C escape to space, is substantially lower than that of the bulk CO_2 atmosphere, suggesting a lower escape fractionation factor than previously thought.*

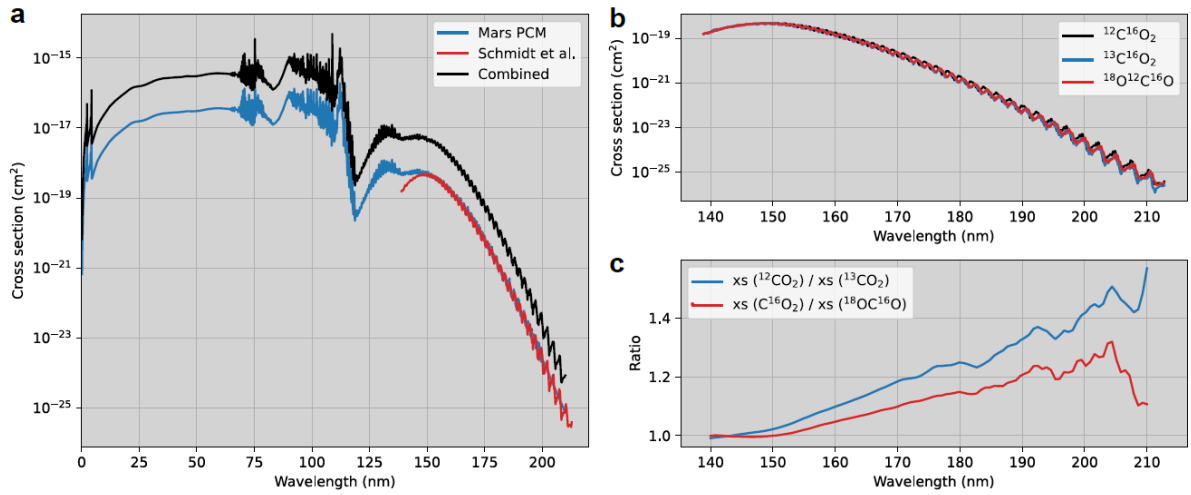

Extended Data Figure 1: Summary of the photolysis cross sections used in this study. *Panel a shows a comparison between the cross sections tabulated in the Mars PCM (blue line) and those calculated by Schmidt et al.[19] (red line) at 295 K. In addition, the combined cross sections used in this study are shown with a x10 offset (black line). Panel b shows the cross sections calculated by Schmidt et al.[19] for the different isotopologues. Panel c shows the ratio between the cross sections of the major and minor isotopes, convolved with a Gaussian function with a FWHM of 2.5nm to smooth out high frequency variations.*

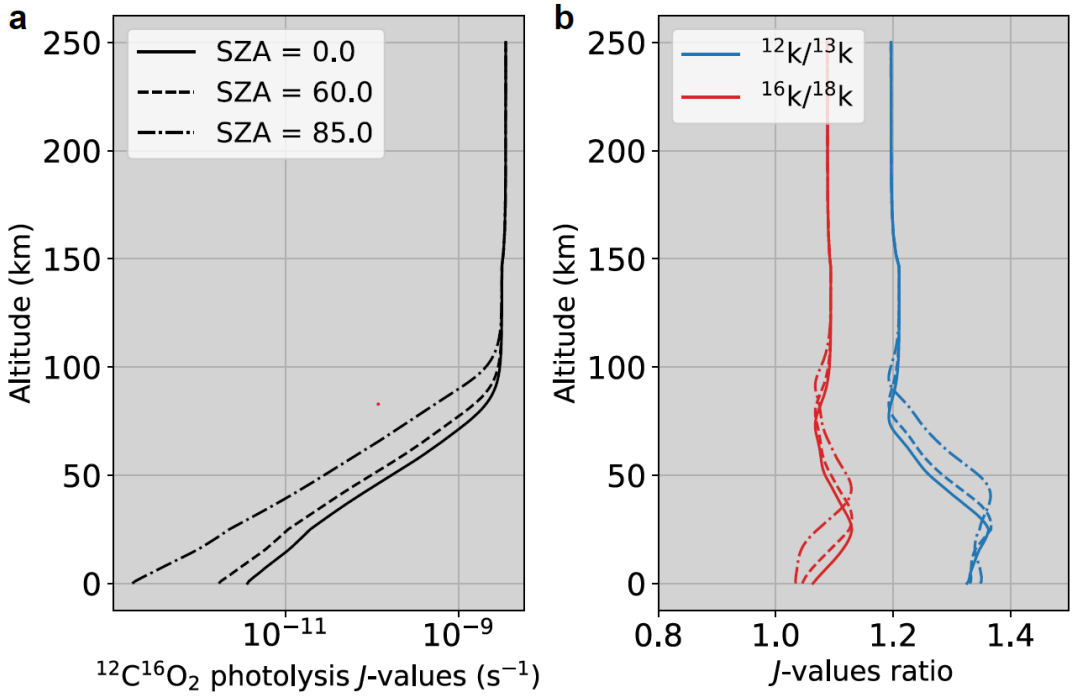

Extended Data Figure 2: Photolysis J-values of $^{12}C^{16}O_2$ and the isotope effect. *Panel a shows the calculated photolysis J-values of $^{12}C^{16}O_2$ at three different solar zenith angles. Panel b shows the ratio between the photolysis rates of $^{12}C^{16}O_2$ over those of $^{13}C^{16}O_2$ and $^{18}O^{12}C^{16}O$.*

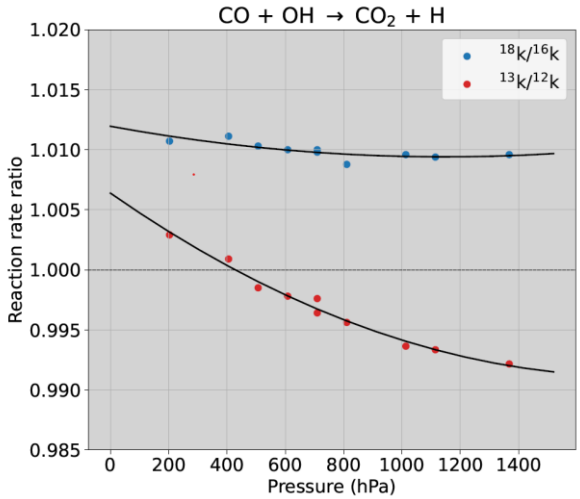

Extended Data Figure 3: Isotopic fractionation during the recombination of CO and OH into CO_2 and H. *The blue and red dots represent the ratio between the reaction rates of $C^{18}O/C^{16}O$ and $^{13}CO/^{12}CO$, measured by Stevens et al.[25]. The black lines are a second-order polynomial fit used to capture the pressure dependence of this fractionation effect. Values of $^{18}k/^{16}k = 1.012$ and $^{13}k/^{12}k = 1.006$ are applicable to the conditions of the Martian atmosphere.*

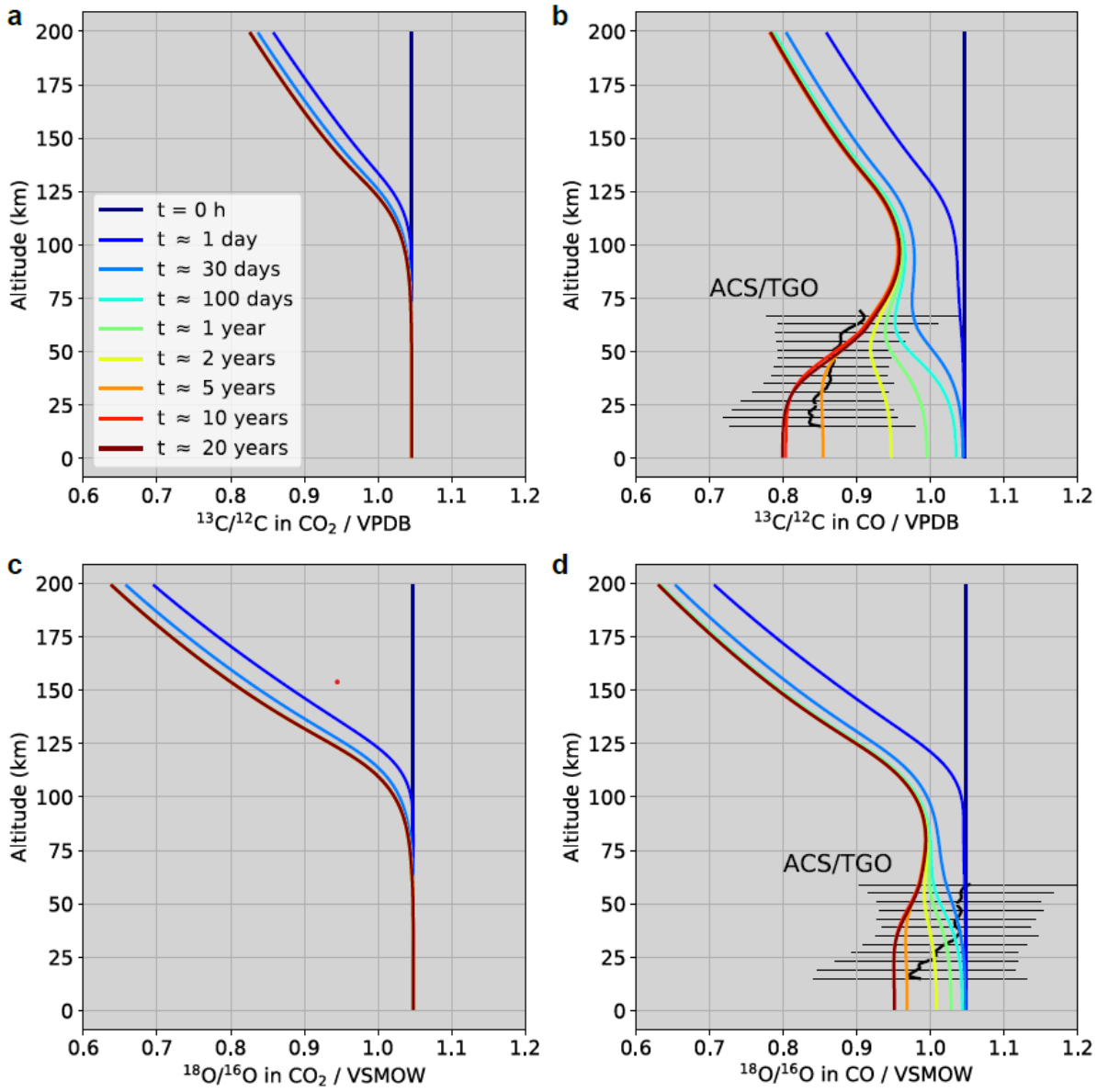

Extended Data Figure 4: Evolution of the isotopic ratios in the 1D photochemical model. *The four panels show the carbon (a,b) and oxygen (c,d) isotopic ratios in CO_2 (a,c) and CO (b,d) as a function of time as the simulation from the photochemical model progresses, together with the ACS averaged isotopic ratios in CO with uncertainties lower than 0.15 in standard units (black lines). The isotopic ratios in CO_2 converge rapidly, as they are mostly affected by diffusive separation, which produces a decrease of the isotopic ratios above the homopause according to their own mass-dependent scale heights. The isotopic ratios in CO are affected by both diffusive separation and by the photochemistry-induced fractionation. The photochemistry of the atmosphere produces a depletion in the $^{13}C/^{12}C$ and $^{18}O/^{16}O$ ratios, whose effect is stronger for the former of the two, in line with the ACS observations.*

9. References

1. Baker, V. R. Water and the martian landscape. *Nature* **412**, 228–236 (2001).
2. Head, J. W. *et al.* Possible Ancient Oceans on Mars: Evidence from Mars Orbiter Laser Altimeter Data. *Science* **286**, 2134–2137 (1999).
3. McElroy, M. B., Yung, Y. L. & Nier, A. O. Isotopic Composition of Nitrogen: Implications for the Past History of Mars' Atmosphere. *Science* **194**, 70–72 (1976).
4. Owen, T., Maillard, J. P., de Bergh, C. & Lutz, B. L. Deuterium on Mars: The Abundance of HDO and the Value of D/H. *Science* **240**, 1767–1767 (1988).
5. Hu, R., Kass, D. M., Ehlmann, B. L. & Yung, Y. L. Tracing the fate of carbon and the atmospheric evolution of Mars. *Nature Communications* **6**, 10003 (2015).
6. Hu, R. & Thomas, T. B. A nitrogen-rich atmosphere on ancient Mars consistent with isotopic evolution models. *Nat. Geosci.* **15**, 106–111 (2022).
7. Scheller, E. L., Ehlmann, B. L., Hu, R., Adams, D. J. & Yung, Y. L. Long-term drying of Mars by sequestration of ocean-scale volumes of water in the crust. *Science* eabc7717 (2021) doi:10.1126/science.abc7717.
8. Krasnopolsky, V. A., Mumma, M. J. & Gladstone, G. R. Detection of Atomic Deuterium in the Upper Atmosphere of Mars. *Science* **280**, 1576–1580 (1998).
9. Yung, Y. L. *et al.* HDO in the Martian atmosphere: Implications for the abundance of crustal water. *Icarus* **76**, 146–159 (1988).
10. Webster, C. R. *et al.* Isotope Ratios of H, C, and O in CO2 and H2O of the Martian Atmosphere. *Science* **341**, 260–263 (2013).
11. Mahaffy, P. R. *et al.* Abundance and Isotopic Composition of Gases in the Martian Atmosphere from the Curiosity Rover. *Science* **341**, 263–266 (2013).
12. Fox, J. L. & Hać, A. Velocity distributions of C atoms in CO^+ dissociative recombination: Implications for photochemical escape of C from Mars. *J. Geophys. Res.* **104**, 24729–24737 (1999).
13. Fox, J. L. & Hać, A. Isotope fractionation in the photochemical escape of O from Mars. *Icarus* **208**, 176–191 (2010).
14. Jakosky, B. M. The CO2 inventory on Mars. *Planetary and Space Science* **175**, 52–59 (2019).
15. Cui, J., Wu, X.-S., Gu, H., Jiang, F.-Y. & Wei, Y. Photochemical escape of atomic C and N on Mars: clues from a multi-instrument MAVEN dataset. *A&A* **621**, A23 (2019).
16. Gröller, H., Lichtenegger, H., Lammer, H. & Shematovich, V. I. Hot oxygen and carbon escape from the martian atmosphere. *Planetary and Space Science* **98**, 93–105 (2014).
17. Lo, D. Y., Yelle, R. V., Lillis, R. J. & Deighan, J. I. Carbon photochemical escape rates from the modern Mars atmosphere. *Icarus* **360**, 114371 (2021).
18. House, C. H. *et al.* Depleted carbon isotope compositions observed at Gale crater, Mars. *Proc. Natl. Acad. Sci. U.S.A.* **119**, e2115651119 (2022).
19. Schmidt, J. A., Johnson, M. S. & Schinke, R. Carbon dioxide photolysis from 150 to 210 nm: Singlet and triplet channel dynamics, UV-spectrum, and isotope effects. *Proceedings of the National Academy of Sciences* **110**, 17691–17696 (2013).
20. McElroy, M. B. & Donahue, T. M. Stability of the Martian Atmosphere. *Science* **177**, 986–988 (1972).
21. Parkinson, T. D. & Hunten, D. M. Spectroscopy and Acronomy of O2 on Mars. *Journal of the Atmospheric Sciences* **29**, 1380–1390 (1972).
22. Korablev, O. *et al.* The Atmospheric Chemistry Suite (ACS) of Three Spectrometers for the ExoMars 2016 Trace Gas Orbiter. *Space Sci Rev* **214**, 7 (2018).
23. Fedorova, A. *et al.* Climatology of the CO Vertical Distribution on Mars Based on ACS TGO Measurements. *JGR Planets* **127**, (2022).
24. Olsen, K. S. *et al.* The vertical structure of CO in the Martian atmosphere from the ExoMars Trace Gas Orbiter. *Nat. Geosci.* **14**, 67–71 (2021).
25. Stevens, C. M. *et al.* The kinetic isotope effect for carbon and oxygen in the reaction CO + OH. *Int. J. Chem. Kinet.* **12**, 935–948 (1980).

26. Krasnopolsky, V. A. Solar activity variations of thermospheric temperatures on Mars and a problem of CO in the lower atmosphere. *Icarus* **207**, 638–647 (2010).
27. Alday, J. *et al.* Isotopic Composition of CO_2 in the Atmosphere of Mars: Fractionation by Diffusive Separation Observed by the ExoMars Trace Gas Orbiter. *JGR Planets* **126**, (2021).
28. Cheng, B.-M. *et al.* Photo-induced fractionation of water isotopomers in the Martian atmosphere. *Geophys. Res. Lett.* **26**, 3657–3660 (1999).
29. Krasnopolsky, V. A. Mars' upper atmosphere and ionosphere at low, medium, and high solar activities: Implications for evolution of water. *Journal of Geophysical Research: Planets* **107**, 11–1 (2002).
30. Cangi, E. M., Chaffn, M. S. & Deighan, J. Higher Martian atmospheric temperatures at all altitudes increase the D/H fractionation factor and water loss. *J. Geophys. Res. Planets* **125**, e2020JE006626 (2020).
31. Krasnopolsky, V. A. Variations of the HDO/H2O ratio in the martian atmosphere and loss of water from Mars. *Icarus* **257**, 377–386 (2015).
32. Wright, I. P., Carr, R. H. & Pillinger, C. T. Carbon abundance and isotopic studies of Shergotty and other shergottite meteorites. *Geochimica et Cosmochimica Acta* **50**, 983–991 (1986).
33. Kass, D. M. Change in the Martian atmosphere. (California Institute of Technology, 1999).
34. Jakosky, B. M. *et al.* Loss of the Martian atmosphere to space: Present-day loss rates determined from MAVEN observations and integrated loss through time. *Icarus* **315**, 146–157 (2018).
35. Fox, J. L. & Hać, A. B. Photochemical escape of oxygen from Mars: A comparison of the exobase approximation to a Monte Carlo method. *Icarus* **204**, 527–544 (2009).
36. Irwin, P. G. J. *et al.* The NEMESIS planetary atmosphere radiative transfer and retrieval tool. *Journal of Quantitative Spectroscopy and Radiative Transfer* **109**, 1136–1150 (2008).
37. Alday, J. *et al.* Isotopic fractionation of water and its photolytic products in the atmosphere of Mars. *Nature Astronomy* (2021) doi:10.1038/s41550-021-01389-x.
38. Gordon, I. E. *et al.* The HITRAN2020 molecular spectroscopic database. *Journal of Quantitative Spectroscopy and Radiative Transfer* **277**, 107949 (2022).
39. Alday, J. *et al.* Oxygen isotopic ratios in Martian water vapour observed by ACS MIR on board the ExoMars Trace Gas Orbiter. *A&A* **630**, A91 (2019).
40. Quémerais, E. *et al.* Stellar occultations observed by SPICAM on Mars Express. *J. Geophys. Res.* **111**, E09S04 (2006).
41. Holmes, J. A., Lewis, S. R. & Patel, M. R. OpenMARS: A global record of martian weather from 1999 to 2015. *Planetary and Space Science* **188**, 104962 (2020).
42. Belyaev, D. A. *et al.* Thermal Structure of the Middle and Upper Atmosphere of Mars From ACS/TGO CO_2 Spectroscopy. *JGR Planets* **127**, (2022).
43. Krasnopolsky, V. A. Photochemistry of the Martian Atmosphere (Mean Conditions). *Icarus* **101**, 313–332 (1993).
44. Lefèvre, F. *et al.* Relationship Between the Ozone and Water Vapor Columns on Mars as Observed by SPICAM and Calculated by a Global Climate Model. *JGR Planets* **126**, (2021).
45. Lefèvre, F., Lebonnois, S., Montmessin, F. & Forget, F. Three-dimensional modeling of ozone on Mars. *Journal of Geophysical Research: Planets* **109**, (2004).
46. Cariolle, D. *et al.* ASIS v1.0: an adaptive solver for the simulation of atmospheric chemistry. *Geosci. Model Dev.* **10**, 1467–1485 (2017).
47. Hobbs, R., Shorttle, O., Madhusudhan, N. & Rimmer, P. A chemical kinetics code for modelling exoplanetary atmospheres. *Monthly Notices of the Royal Astronomical Society* **487**, 2242–2261 (2019).
48. Verwer, J. G., Spee, E. J., Blom, J. G. & Hundsdorfer, W. A Second-Order Rosenbrock Method Applied to Photochemical Dispersion Problems. *SIAM J. Sci. Comput.* **20**, 1456–1480 (1999).

49. Forget, F. *et al.* Improved general circulation models of the Martian atmosphere from the surface to above 80 km. *J. Geophys. Res.* **104**, 24155–24175 (1999).
50. Hunten, D. M. The Escape of Light Gases from Planetary Atmospheres. *J. Atmos. Sci.* **30**, 1481–1494 (1973).
51. Chaffin, M. S., Deighan, J., Schneider, N. M. & Stewart, A. I. F. Elevated atmospheric escape of atomic hydrogen from Mars induced by high-altitude water. *Nature Geosci* **10**, 174–178 (2017).
52. Huestis, D. L. & Berkowitz, J. Critical Evaluation of the Photoabsorption Cross Section of CO2 from 0.125 to 201.6 nm at Room Temperature. **42**, 48.13 (2010).
53. Lewis, B. R. & Carver, J. H. Temperature dependence of the carbon dioxide photoabsorption cross section between 1200 and 1970 Å. *Journal of Quantitative Spectroscopy and Radiative Transfer* **30**, 297–309 (1983).
54. Parkinson, W. H., Rufus, J. & Yoshino, K. Absolute absorption cross section measurements of in the wavelength region 163–200 nm and the temperature dependence. *Chemical Physics* **290**, 251–256 (2003).
55. Stark, G., Yoshino, K., Smith, P. L. & Ito, K. Photoabsorption cross section measurements of CO2 between 106.1 and 118.7nm at 295 and 195K. *Journal of Quantitative Spectroscopy and Radiative Transfer* **103**, 67–73 (2007).
56. Yoshino, K. *et al.* Absorption cross section measurements of carbon dioxide in the wavelength region 118.7–175.5 nm and the temperature dependence. *Journal of Quantitative Spectroscopy and Radiative Transfer* **55**, 53–60 (1996).
57. Alday, J. Isotopic composition of CO, CO2 and H2O in the atmosphere of Mars from ACS/TGO. (2023) doi:10.5281/ZENODO.7499466.
58. Irwin, P. nemesiscode/radtrancode: NEMESIS. (2022) doi:10.5281/ZENODO.5816714.
59. Alday, J. juanaldayparejo/pchempy-dist: 1D Photochemical Model with Isotopic Fractionation for Mars' atmosphere. (2023) doi:10.5281/ZENODO.7807731.